A&A 430, 853–864 (2005)
DOI: 10.1051/0004-6361:20041566
© ESO 2005

Astronomy & Astrophysics

# Detecting cold $H_2$ globules in the outer Galactic disc by microlensing towards the Maffei 1 elliptical

R. Fux

Geneva Observatory, Ch. des Maillettes 51, 1290 Sauverny, Switzerland
e-mail: Roger.Fux@obs.unige.ch

Received 30 June 2004 / Accepted 20 September 2004

**Abstract.** A candidate source of dark matter in spiral galaxies is cold molecular hydrogen globules with a condensed central core and a disc-like space distribution probably similar to that of neutral hydrogen. This paper shows that the $H_2$ cores are sufficiently compact and massive to be detected by microlensing in the outer Galactic disc and that the Maffei 1 elliptical galaxy, at a distance of 3 Mpc and Galactic latitude $b = -0.6°$, offers an ideal target for such an experiment. The microlensing optical depth of $H_2$ cores along the line of sight to this galaxy is estimated to $\tau \sim 0.7 \times 10^{-6}$ if most of the dark mass in the Milky Way resides in such cores, and the typical event timescale to $\lesssim$1 day. Detection rates are computed both in the classical and pixel lensing approaches in the $I$- and $K$-bands, and for a representative selection of existing observing facilities. In the more efficient pixel lensing case, two 10-h observing runs, separated in time by at least several days, should yield of the order of 10 positive detections at the $5\sigma$ level using ground-based 8 m-class telescopes in the $K$-band or the Hubble Space Telescope ACS camera in the $I$-band, and the corresponding fraction of events with timescale measurable to an accuracy better than 50% amounts to about 9% and 4% respectively for these observing alternatives.

**Key words.** cosmology: dark matter – Galaxy: disk – ISM: molecules – gravitational lensing – methods: observational

## 1. Introduction

The nature of dark matter (DM) in the universe is one of the main persistent problems in modern astrophysics. In spiral galaxies, dark matter is highlighted by flat HI rotation curves extending far beyond the optical disc, where one would expect a Keplerian fall-off (e.g. Rogstad & Shostak 1972). Many DM candidates have been proposed in the literature, including massive compact objects, neutrinos and other more exotic particles. Compact objects have been and are still searched for in the local group using classical or pixel microlensing of stellar sources located in the Galactic bulge, the Magellanic Clouds and Andromeda (e.g. the OGLE, MACHO, EROS, MOA, AGAPEROS, MEGA, POINT-AGAPE, WeCAPP collaborations[1]). All these experiments are designed to find dark objects in the inner Galaxy or in the more or less spherical halos around the Milky Way and Andromeda galaxies.

An attractive possible constituent of galactic DM is $H_2$ in the form of cold "globules", made of a condensed solid or liquid central core surrounded by an extended atmosphere (Pfenniger 2004; Pfenniger & Combes 1994; see also White 1996). These $H_2$ cores would have radii of up to $2 \times 10^4$ km and masses up to the Earth mass. A number of constraints, like the HI–DM relation (Bosma 1981), the disc-halo conspiracy, the maximum disc property implying hollow spherical halos, and the large angular momentum of accreted high velocity clouds, do support a space distribution of $H_2$ globules similar to the HI distribution, i.e. as an outer disc around spiral galaxies. Evidence for large amounts of molecular gas in such regions is also provided by the observed star formation in the extreme outskirts of the HI disc in M 31 (Cuillandre et al. 2001). Moreover, $N$-body simulations show that massive collisionless DM discs are prone to bending instabilities leading to long lasting warps (Revaz & Pfenniger 2004), consistent with the observed high frequency of these structures.

This paper shows that if $H_2$ cores contain most of the Milky Way's DM and have a disc-like distribution, they should be quite easily detectable through a short microlensing experiment targeting the low Galactic latitude Maffei 1 galaxy.

The structure of the paper is as follow. Section 2 summarises the main observational characteristics of Maffei 1. Section 3 briefly outlines the microlensing aspects useful to our investigation and evaluates the basic properties resulting from the lensing of extragalactic sources by $H_2$ cores. Section 4 introduces the concept of fluctuation magnitude and attempts to derive a realistic stellar luminosity function for Maffei 1. Section 5 then computes the expected event detection rates for a representative set of available observational facilities, both in the classical and pixel lensing workframes. Finally, Sect. 6 argues that a massive Galactic $H_2$-globule disc is not excluded by current microlensing constraints, and Sect. 7 concludes the paper. The problem of contamination by variable stars is

[1] See respectively Wozniak et al. (2001), Alcock et al. (1998), Afonso et al. (2003), Bond et al. (2001), Melchior et al. (1998), de Jong et al. (2004), Paulin-Henriksson et al. (2003), and Riffeser et al. (2003), for selected references.

Article published by EDP Sciences and available at http://www.aanda.org or http://dx.doi.org/10.1051/0004-6361:20041566

**Fig. 1.** *JHK* composite image of Maffei 1 from the 2MASS Large Galaxy Atlas (Jarrett et al. 2003). The field of view is $11.9' \times 11.9'$.

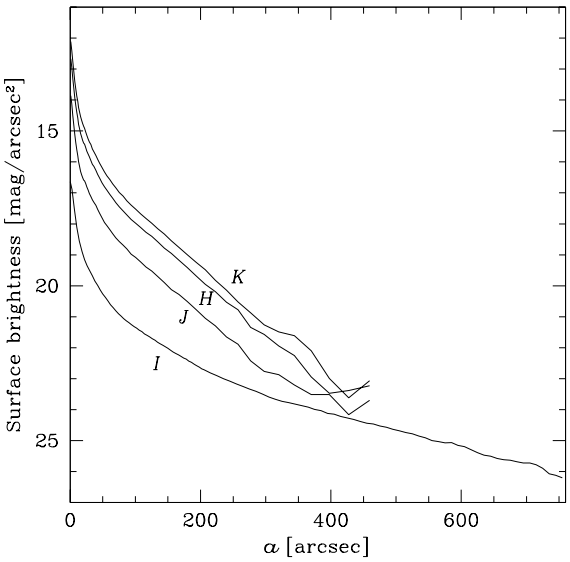


**Fig. 2.** Radial surface brightness profile of Maffei 1 in *IJHK* along the galaxy major axis. The *I*-band data are from Buta & McCall (1999) and the *JHK* data from the 2MASS Large Galaxy Atlas (Jarrett et al. 2003). The shifts between the curves partly reflect the chromatic extinction.

beyond the scope of this paper and will not be treated, and the case of more diffuse $H_2$ clouds is analysed in Rafikov & Draine (2001). Much of the notations and theory elements are based on Gould (1996; hereafter G96).

## 2. The Maffei 1 galaxy

With a distance of only 3 Mpc and an extinction corrected *I*-band luminosity of $M_I = -22$ mag (Fingerhut et al. (2003), Maffei 1 is the nearest normal giant elliptical galaxy to the Milky Way. Its apparent size on the sky is about 2/3 that of the full moon. Moreover, with Galactic coordinates $(\ell, b) = (135.9°, -0.6°)$, this galaxy lies very close to the Galactic plane and hence represents an excellent target for a microlensing search of compact objects in the outer Galactic disc. Maffei 1 has been fairly well studied in the recent past. Figure 1 shows the near-IR aspect of the galaxy and Fig. 2 its radial profile in several photometric bands. The large range in surface brightness will prove very convenient for optimising the classical lensing detection rates. The high extinction by dust inherent to low latitude objects amounts to $A_I = 2.64$ mag in the optical towards Maffei 1 (Buta & McCall 1999), but is reduced to $A_K = 0.57$ mag in the near-IR (Fingerhut et al. 2003). The equatorial coordinates $\alpha = 02{:}36{:}35.4$, $\delta = +59{:}39{:}16.5$ (J2000) mean that ground-based observations of Maffei 1 have to be done from the northern hemisphere and that the optimal period is around October−November. During this period and if observing from Mauna Kea at a geographic latitude of +19°, Maffei 1 is about 9 and 10 h at airmass less than 2.1 and 2.4 respectively.

Reported values for the mean isophotal axis ratio and position angle measured eastward from north are respectively 0.73 and 83.9° in the *I*-band (Buta & McCall 1999), and 0.79 and 85.5° in the *K*-band (Jarrett et al. 2003). Hence the apparent principal axes of Maffei 1 nearly coincide with the $\alpha$ and $\delta$ coordinate axes.

Maffei 1 is part of the Maffei group, which also contains another large galaxy known as Maffei 2. This is a spiral galaxy which lies even closer to the Galactic plane, at $b = -0.3°$, and thus provides another possible target which will not be considered here.

## 3. Basic microlensing properties

This section briefly reviews the light curves associated with microlensing events, and evaluates the typical Einstein radius, microlensing optical depth and timescale for the lensing of extragalactic sources by $H_2$ cores in the outer Galactic disc.

### 3.1. Light curves

Microlensing of a stellar source is the amplification of its measured flux due to foreground lensing objects passing close to its line of sight. If $\theta$ is the angular separation of the lens relative to the source, the magnification factor for a point source is given by:

$$A(x) = \frac{x^2+2}{x\sqrt{x^2+4}}, \qquad x \equiv \theta/\theta_{\rm E}, \tag{1}$$

where $\theta_{\rm E} \equiv r_{\rm E}/D_{\rm L}$ is the apparent radius of the Einstein ring (see Sect. 3.2). The motion of the lens with respect to the line of sight to the source is generally well approximated by a uniform velocity $\boldsymbol{v}$, and thus:

$$x(t; t_0, \beta, \omega) = \sqrt{\omega^2(t-t_0)^2 + \beta^2}, \tag{2}$$

where $t_0$ is the time of maximum magnification, $\beta = x_{\rm min}$ the impact parameter in units of $\theta_{\rm E}$ and $\omega^{-1} \equiv r_{\rm E}/v$ the half timescale.

As discussed in G96, the truly measurable quantity in crowded fields is not the magnification itself, but the excess flux $F(A-1)$, where $F$ is the unmagnified flux of the lensed

star. And for small impact parameters ($\beta \ll 1$) and near the maximum magnification ($|\omega(t-t_0)| \ll 1$), this excess flux takes the limiting form:

$$F[A(t;t_0,\beta,\omega)-1] \rightarrow \frac{F}{\beta} G(t;,t_0,\omega_{\rm eff}), \tag{3}$$

where

$$G(t;,t_0,\omega_{\rm eff}) \equiv \frac{1}{\sqrt{\omega_{\rm eff}^2 (t-t_0)^2+1}} \tag{4}$$

and $\omega_{\rm eff} \equiv \omega/\beta$. Hence, in the case where the intrinsic signal of the source star is well below the background noise and the event detectable only through high amplification, i.e. small $\beta$, only $F/\beta$ and $\omega_{\rm eff}$ can be constrained. This is the so called "spike" regime of pixel lensing. Measuring individually all the $F, \beta$ and $\omega$ parameters requires the wings of the light curve.

### 3.2. Einstein radius

In the case of extragalactic stars lensed by $H_2$ cores in the outer Galactic disc, the absolute Einstein radius is:

$$r_{\rm E} = 2.3 \times 10^6 \ {\rm km} \left(\frac{m_{\rm L}}{M_\oplus}\right)^{1/2} \left[\frac{D_{\rm L}}{10 \ {\rm kpc}} \cdot \frac{D_{\rm S}-D_{\rm L}}{D_{\rm S}}\right]^{1/2} \tag{5}$$

(or 3.4 $R_\odot$), where $m_{\rm L}$ is the mass of the cores, $M_\oplus = 3.0 \times 10^{-6}\ M_\odot$ the Earth mass, and $D_{\rm S}$ and $D_{\rm L}$ are the distances of the source and the lens respectively. For sources in the Maffei group, $(D_{\rm S}-D_{\rm L})/D_{\rm S} \approx 1$. Hence $r_{\rm E}$ is typically two orders of magnitude larger than the maximum radius of the $H_2$ cores, ensuring that the cores are sufficiently compact for the above formula to be applicable. Moreover, at the distance of the Maffei group, the apparent Einstein radius of the cores represents a transverse distance $(D_{\rm S}/D_{\rm L}) r_{\rm E} \approx 850\ R_\odot$, large enough to consider even the brightest stars as point sources for not too small impact parameters. More quantitatively, for sources of finite apparent radius $\theta_{\rm S}$, Gould (1995b) has shown that the true magnification *exceeds* the point source magnification of Eq. (1) by up to ~25% as long as $\beta \gtrsim 0.5\theta_{\rm S}/\theta_{\rm E}$. Near the tip of the red giant branch, the stars have a radius of about 100 $R_\odot$, which means that Eq. (1) provides a useful lower limit for at least $\beta \gtrsim 0.06$.

### 3.3. Microlensing optical depth

The microlensing optical depth $\tau$ towards a source star is the probability that this star lies within the apparent Einstein radius of any intervening lens, i.e. that its flux is magnified by at least ~0.32 mag.

To estimate the optical depth towards extragalactic sources due to Galactic $H_2$ cores, we make the following assumptions: (i) most of the $H_2$ globule mass is contained in the condensed core; (ii) the space distribution of the globules is similar to that of the HI gas, as justified in Sect. 1; and (iii) the $H_2$ globules represent twice the HI mass. This last assumption is based on the fact that the scatter in the Tully-Fisher relation for external galaxies is significantly reduced if the contribution of the HI mass is multiplied by a factor up to 3, and not anymore for larger factors (Pfenniger, private communication). For the Milky Way, this is a rather pessimistic assumption if $H_2$ is to make most of the Galactic dark mass. Indeed, adding 3 times the HI mass distribution to the stellar mass distribution is insufficient to rise the rotation curve above 190 km s$^{-1}$ in the outer disc. This may however compensate to some extent the optimistic first assumption.

Resorting to the available HI data cubes, the traditional integral over $D_{\rm L}$ that defines the microlensing optical depth can be converted into a sum over the velocity bins:

$$\tau = \frac{4\pi G\, X m_{\rm p}\, \gamma}{c^2} \cdot \sum_{\substack{i \\ 0 \le D_i \le D_{\rm S}}} T_{\rm b}(V_i) D_i \frac{D_{\rm S}-D_i}{D_{\rm S}} \Delta V, \tag{6}$$

where $T_{\rm b}$ is the brightness temperature, $\Delta V$ the velocity resolution element, $V_i$ the velocity in the $i$th bin, $D_i$ the distance corresponding to this velocity, $X$ the conversion factor of $T_{\rm b}$ into HI atom column density per unit velocity ($X = 1.823 \times 10^{22}$ in MKSA units, see Burton 1992), $\gamma = 2$ the assumed $H_2$/HI mass ratio, and $m_{\rm p}$ the proton mass. To infer $D_i$ from $V_i$, a simple kinematic model where the Sun and the HI gas move on circular orbits with constant circular velocity $v_{\rm c}(R) = v_0 = 200$ km s$^{-1}$ and the galactocentric distance of the Sun $R_0 = 8$ kpc is adopted. The computed optical depths only marginally depend on the chosen model. The contribution of the inner Galaxy, complicated by the well known near and far side distance degeneracy relative to the tangent point, is not of special interest here and is therefore discarded.

The resulting microlensing optical depth map is shown in Fig. 3. The advantage of our procedure is that it takes fully account of the deviations of the HI disc from the $b = 0$ plane. The $H_2$-core optical depth can reach values as high as $\tau_{-6} = 1$, where $\tau_{-6}$ is the optical depth expressed in units of $10^{-6}$. This is nearly as much as the values of ~2 measured by the microlensing experiments towards the Galactic bulge (e.g. Popowski et al. 2001). In the direction of Maffei 1, $\tau_{-6} \approx 0.7$, very close to these maximum values. Note that $\tau$ does depend neither on $m_{\rm L}$ for compact lenses, nor on the lens velocity distribution.

### 3.4. Timescale

With the same kinematic model as used in the former section, assuming that the Sun and the $H_2$ globules are on circular orbits and neglecting the proper motion of the Maffei 1 stars relative to the Galactic centre, the transverse velocity of the globules relative to these stars line of sight is:

$$v = \left[\sqrt{1 - \frac{\sin^2 \ell}{1 - 2D_{\rm L}/R_0 \cos\ell + (D_{\rm L}/R_0)^2}} + \cos\ell\right] \cdot v_0, \tag{7}$$

where $\ell$ is the Galactic longitude of Maffei 1. In particular, for $D_{\rm L} = 10$ kpc, one gets $v = 0.225 v_0 = 45$ km s$^{-1}$. The Earth's motion relative to the Sun adds a quasi constant velocity of about 17 km s$^{-1}$ in October-November, which is around the yearly maximum value, and the Sun's motion relative to the LSR about $-11$ km s$^{-1}$, implying a resulting $v \approx 50$ km s$^{-1}$. At such a transverse velocity, the timescale of a microlensing

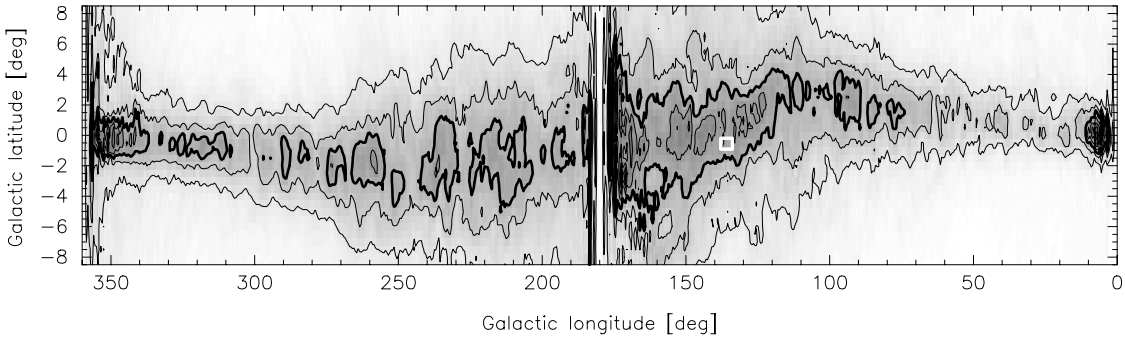


**Fig. 3.** Microlensing optical depth map near the Galactic plane of the $H_2$ globule cores assuming that their 3D mass density is twice that of the observed neutral hydrogen, for distant extragalactic sources ($D_S \gg D_L$). The contours are spaced by $\Delta\tau_{-6} = 0.2$ and the thick contour stands for $\tau_{-6} = 0.6$. The location of Maffei 1 is indicated by the white square. The HI data are from Hartmann & Burton (1997), Burton & Liszt (1978) and Kerr et al. (1967).

event, corresponding to the crossing time of the Einstein ring, amounts to:

$$2\omega^{-1} \equiv \frac{2r_E}{v} = 26.0\, h \left(\frac{r_E}{3.4\, R_\odot}\right)\left(\frac{50\ \mathrm{km\ s^{-1}}}{v}\right). \quad (8)$$

Hence one observing night enables to measure at least the third of a lensing light curve if $m_L \lesssim 1\ M_\oplus$, but it may not be possible to get the full curve from a single ground-based telescope. According to Eq. (5), $\omega^{-1} \propto \sqrt{m_L}$, and thus the timescale decreases with lens mass.

Equation (5) also leads to $\omega^{-1} \propto \sqrt{D_L}/v$ at fixed lens mass, which for the simple mean velocity model expressed in Eq. (7), implies that the timescale is constant to within about 10% in the distance range 2 kpc $\lesssim D_L \lesssim$ 10 kpc and significantly increases only at shorter distances.

## 4. Luminosity function and fluctuation magnitude

In order to calculate detection rates, we will need to quantify the surface brightness noise due to the finite number of stars in a galaxy, and specify a realistic stellar luminosity function $\Phi(F)$ applicable to the Maffei 1 galaxy.

The surface brightness noise is conveniently characterised by the "fluctuation flux", which is defined as the ratio of the second to the first moments of the luminosity function:

$$F_* \equiv \frac{\int_0^\infty \Phi(F) F^2 \mathrm{d}F}{\int_0^\infty \Phi(F) F \mathrm{d}F}. \quad (9)$$

This flux, which is also fundamental to the surface brightness fluctuation method for measuring distances, represents the flux of the stars in a system made of identical stars that would statistically produce the same surface brightness profile and the same surface brightness fluctuation as the real stellar system.

The observed absolute fluctuation magnitudes of galaxies in $IHK$ as a function of intrinsic colour are:

$$\bar{M}_I = (-1.74 \pm 0.07) + (4.5 \pm 0.25)[(V-I)_0 - 1.15] \quad (10)$$

(Tonry et al. 1997),

$$\bar{M}_H = (-5.03 \pm 0.03) + (5.1 \pm 0.5)[(V-I)_0 - 1.16] \quad (11)$$

(Jensen et al. 2003),

$$\bar{M}_{K_s} = (-5.84 \pm 0.04) + (3.6 \pm 0.8)[(V-I_C)_0 - 1.15] \quad (12)$$

(Liu et al. 2002).

Fingerhut et al. (2003) report $(V-I)_0 = 1.06 \pm 0.09$ for Maffei 1, which implies $\bar{M}_I = -2.1$ and $\bar{M}_{K_s} = -6.2$ for this galaxy. The agreement with the theoretical values derived from population synthesis models is very good in the $I$-band, but not in the $K$-band, where the models predict $\bar{M}_K = -4.9$ (Cantiello et al. 2003). The fact is that the fluctuation magnitude is much brighter in the near-IR than in the optical.

The stellar luminosity functions of nearby galaxies show a power law behaviour at the bright end over a large range of magnitude (apart from the red clump bump), with a rather sharp cut-off at the tip of the red giant branch and a flattening at fainter magnitudes. In this paper, we will use the following functional form:

$$\Phi(F) = \begin{cases} 0 & F > F_{\mathrm{lim}}, \\ \dfrac{C}{F^n} & F_0 \le F \le F_{\mathrm{lim}}, \\ w\dfrac{C}{F_0^n} & F \le F_0, \end{cases} \quad (13)$$

where the variable $F$ is the observed flux, $F_{\mathrm{lim}}$ the bright end cut-off flux, $F_0$ the "knee" flux where the power law breaks and $\Phi(F)$ flattens, and $w$ a parameter to tune the contribution of faint stars. Our results will only marginally depend on the precise choice of this last parameter and we therefore arbitrarily set $w = 0$. If $n \neq 1$, the normalisation factor is:

$$C = \frac{(n-1)(F_{\mathrm{lim}}F_0)^{n-1}}{[1+(n-1)w]F_{\mathrm{lim}}^{n-1} - F_0^{n-1}}. \quad (14)$$

In the realistic case $F_0 \ll F_{\mathrm{lim}}$, the resulting absolute fluctuation magnitude is well approximated by:

$$\bar{M} = \begin{cases} M_{\mathrm{lim}} + 2.5 \log\left[\nu(M_0 - M_{\mathrm{lim}}) + \dfrac{w}{2}\right] & n = 2, \\ M_{\mathrm{lim}} + 2.5 \log\left(\dfrac{3-n}{2-n}\right) & n < 2-\epsilon, \end{cases} \quad (15)$$

where the subscripted absolute magnitudes correspond to the similarly subscripted fluxes, $\nu = 0.4 \ln 10$, and $\epsilon$ is a small non-zero positive number introduced because the given approximation fails when $n \to 2$.

The parameters of $\Phi(F)$ are determined as follow, assuming that Maffei 1 and the bulge of the Milky Way have similar luminosity functions. In the $I$-band, the slope

**Table 1.** Parameters of the adopted *I*- and *K*-band luminosity functions, and the resulting fluctuation magnitudes.

| | Filter | |
|---|---|---|
| | *I* | *K* |
| $n$ | 2.0 | 1.675 |
| $M_{\rm lim}$ | −4.1 | −7.5 |
| $M_0$ | 3.0 | $\infty$ |
| $\bar{M}$ | −2.1 | −6.0 |

of the observed magnitude function in the Galactic bulge is $s \equiv \mathrm{d}\log_{10}\Phi(m)/\mathrm{d}m = 0.4$ for the bright stars (Terndrup et al. 1990), thus $n = 2.5 \cdot s + 1 = 2$. Note that this value differs from $n = 1$ assumed in G96. Here the term +1 arises because $\mathrm{d}F/\mathrm{d}m \propto F$. The tip of the red giant branch lies at $M_{\rm lim} \approx -4.1$ (e.g. Karachentsev et al. 2003) and the knee magnitude at $M_0 \approx 3.0$ (Holtzman et al. 1998), and for these values Eq. (15) yields $\bar{M} = -2.1$, in perfect agreement with the expected fluctuation magnitude of Maffei 1. The agreement would be slightly worse for $w = 1$, probably because our luminosity function ignores supergiants brighter than $M_{\rm lim}$.

In the *K*-band, the observed bright-end slope in the Galactic bulge is $s = 0.27 \pm 0.03$ down to the faintest detected stars, leading to $n = 1.675$, and $M_{\rm lim} \approx -7.5$ (Tiede et al. 1995). For such a value of $n$, Eq. (15) predicts no significant dependence of $\bar{M}$ on $M_0$, so that we arbitrarily chose $M_0 = \infty$, and one gets $\bar{M} = -6.0$, consistent with the quoted value based on observations. Note that $\Phi(F)$ is not normalisable for this choice of $M_0$, but $\bar{M}$ is nevertheless well defined. Table 1 lists the retained values of the parameters.

Finally, we will also need to know the number of stars per unit solid angle and per unit galaxy surface brightness with flux larger than $F$, which for our luminosity function and for $F_0 \leq F \leq F_{\rm lim}$, if $F_0 \ll F_{\rm lim}$ and $1 < n < 3-\epsilon$, is:

$$N(F) = \frac{1}{(n-1)(3-n)} \frac{F_*}{F_{\rm lim}^2} \left[ \left( \frac{F_{\rm lim}}{F} \right)^{n-1} - 1 \right], \tag{16}$$

where $\epsilon$ is as above.

## 5. Detection rates

In this section, we will derive estimates of the expected detection rates of the $H_2$-core microlensing events when targeting the Maffei 1 galaxy with existing observing facilities, assuming $\tau_{-6} = 0.7$ and $\omega^{-1} = 13$ h, as estimated in Sect. 3, and a homogeneous stellar population with $\Phi(F)$ as detailed in Sect. 4. Both classical lensing and pixel lensing approaches are investigated, and the results are presented for one optical and one near-IR filter, i.e. for the *I*- and *K*-bands.

### 5.1. Classical lensing

Classical lensing is the microlensing of sources that are resolved even when not magnified. In this case the source counts contribute significantly to the noise and the signal-to-noise ratio of a star in a given exposure is:

$$Q = \frac{(\alpha F) t_{\rm exp}}{\sqrt{(\alpha F) t_{\rm exp} + \Omega_{\rm psf} \{ (\alpha S)[1 + g(\alpha F_*) t_{\rm exp}] + (\alpha S_{\rm sky}) \} t_{\rm exp}}} \tag{17}$$

where $F$ is the flux from the star, $S$ the galaxy surface brightness, $S_{\rm sky}$ the sky surface brightness including the instrument background, $t_{\rm exp}$ the exposure time, $\Omega_{\rm psf}$ the solid angle covered by the point spread function (PSF), $F_*$ the galaxy fluctuation flux, and $\alpha$ the number of electrons counted by the detector per unit time and unit flux. If $m$ is the apparent magnitude of the star and $Z$ the detector zeropoint, i.e. the magnitude of a star producing one electron per second, then $\alpha F = 10^{0.4(Z-m)}$.

The term $\Omega_{\rm psf}(\alpha S)(\alpha F_*) t_{\rm exp}^2$ represents the fluctuation flux contribution to the squared noise if the background stars were seen as point-like, and the factor $g$ is a correction taking into account the finite seeing:

$$g \equiv \frac{1}{\Omega_{\rm psf}} \int \left[ \int_{\Omega_{\rm psf}} f(\boldsymbol{x}' - \boldsymbol{x}) \mathrm{d}\boldsymbol{x}' \right]^2 \mathrm{d}\boldsymbol{x}, \tag{18}$$

where $f(\boldsymbol{x})$ is the PSF. We will consider $\Omega_{\rm psf} = \pi \theta_{\rm see}^2$, with the seeing $\theta_{\rm see}$ defined as the PSF full width at half maximum. For a Gaussian PSF with standard deviation $\sigma$, $\theta_{\rm see} = 2\sqrt{\ln 4}\sigma$ and $g = 0.544$.

Equation (17) can easily be inverted to get the minimum flux $F_{\rm min}(S, t_{\rm exp})$ necessary to detect a star with a given signal-to-noise threshold $Q > Q_{\rm min}$. This flux is of course a function of the exposure time, but cannot reach arbitrarily small values as $t_{\rm exp} \to \infty$. The fluctuation noise indeed imposes the lower limit:

$$F_{\rm min}(S, \infty) = Q_{\rm min} \sqrt{g \Omega_{\rm psf} (\alpha S)(\alpha F_*)}. \tag{19}$$

The total number of resolvable stars per unit solid angle then amounts to:

$$N_{\rm res}(S, t_{\rm exp}) = S\, N(F_{\rm min}), \tag{20}$$

where $N(F)$ is given by Eq. (16). Now the classical event rate for one star is:

$$\Gamma_0 = \frac{2}{\pi} \omega \tau, \tag{21}$$

thus the number of lensing events per unit solid angle with peak magnification within an observing time interval $\Delta t$ will be:

$$N_{\rm det} = N_{\rm res} \Gamma_0 \Delta t = \frac{2}{\pi} \tau\, S\, N(F_{\rm min})\, \omega \Delta t. \tag{22}$$

Figure 4 displays $N_{\rm res}$ for Maffei 1 as a function of distance from the galaxy centre when observations are carried out in the *I*-band with the ACS camera on the Hubble Space Telescope (HST), and in the *K*-band with the NIRI plus adaptive optic instruments on the Gemini North telescope, assuming $Q_{\rm min} = 3$. Extinction is taken into account, with the values of $A_I$ and $A_K$ mentioned in Sect. 2. The choice of $Q_{\rm min}$ is rather small, but since the same field is observed several times, one can stack the exposures to enhance the signal-to-noise ratio and hence avoid false star detections.

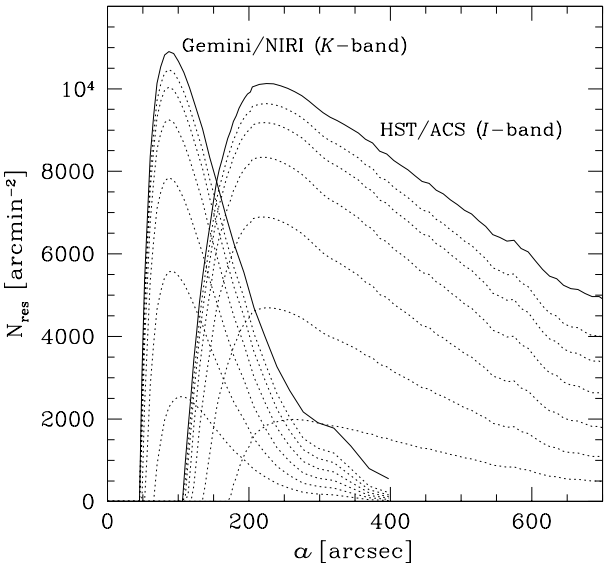


**Fig. 4.** Expected number of resolvable stars per unit solid angle in Maffei 1 as a function of angular radius $a$ along the major axis of the galaxy and exposure time, for two combinations of telescopes and detectors, including adaptive optics in the $K$-band, and using the surface brightness profiles plotted in Fig. 2. The dotted lines are for $t_{\rm exp} = 1, 2, 4, 8, 16, 32$ s for Gemini/NIRI, and for $t_{\rm exp} = 1.25, 2.5, 5, 10, 20, 40$ min for HST/ACS, and the solid lines represent the upper limits resulting from Eq. (19). The detection threshold is set to 3 sigmas. The adopted telescope zeropoints, sky backgrounds and seeing angles are listed in Table 2.

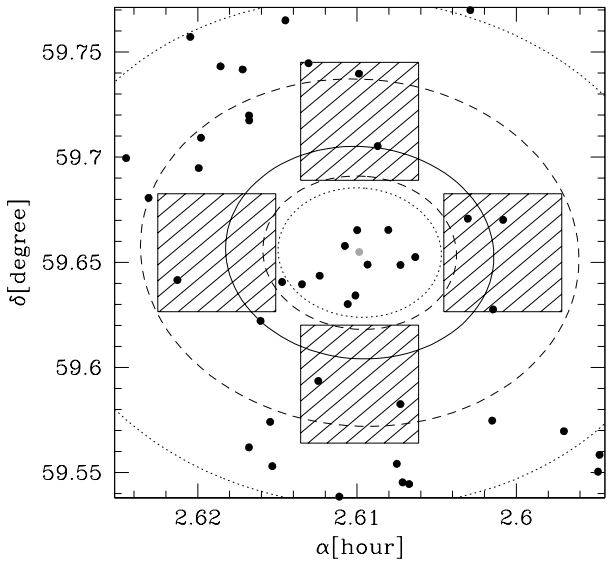


**Fig. 5.** Location of four optimal HST/ACS fields in Maffei 1 for the search of classical lensing events. The full, dashed and dotted lines represent the isophotes where the $I$-band surface density of resolvable stars $N_{\rm res}$ is maximum, 80% of maximum, and 50% of maximum respectively. The dots represent bright guide stars for near-IR adaptive optic observations, obtained from the STSI Guide Star Catalogue I.

The number of resolvable stars increases linearly at low $t_{\rm exp}$ and saturates at large $t_{\rm exp}$ due to the minimum flux limit provided by Eq. (19). The exposure time at the transition between the two regimes is around 10 min for HST/ACS and only 5 s for Gemini/NIRI. For longer exposures, doubling $t_{\rm exp}$ does not efficiently increase $N_{\rm res}$ any further. The shorter integration time required with NIRI comes from the higher values of $S$ and $F_*$, and the lower extinction in $K$, even if the sky is much brighter in this band than in the $I$-band.

In both the HST/ACS and Gemini/NIRI cases, there exists an optimal radius which maximises the number of resolvable stars. Near the centre, the fluctuation noise is so high that $F_{\rm min} > F_{\rm lim}$, preventing the detection of individual stars. This is consistent with the fact that no stars are resolved in Buta & McCall's (2003) HST data of the central region of Maffei 1. At increasing distance, $F_{\rm min}$ decreases below $F_{\rm lim}$ and $N_{\rm res}$ begins to rise abruptly. But at even larger distance, this trend reverses due to the decline with $S$ of the stellar number density. The radius of maximum $N_{\rm res}$ does not vary much with exposure time, except at the short exposure end, where it increases with decreasing $t_{\rm exp}$, and is smaller in $K$ than in $I$ mainly because of the strong chromatic dependence of the luminosity function.

For HST/ACS, the optimum distance along the major axis is around 230 arcsec from the centre. At this radius, if $\Omega$ is the solid angle covered by the detector (see Table 2) and $t_{\rm exp} = 10$ min, one should be able to resolve as many as $\Omega N_{\rm res} \approx 90\,000$ stars, yielding $N_{\rm det} \approx 0.003(\Delta t/{\rm h})$. This is a rather low detection rate that would require many days of HST time if one restricts the observations to a single field. However, thanks to the large apparent size of Maffei 1 and as suggested in G96, the situation can be improved when observing several fields simultaneously. If we require at least 8 exposures per field during the typical half lensing timescale of 13 h, this implies one exposure per field every 96 h of HST orbital time. Given the 56 h visibility period of Maffei 1, the 10.1 min of overhead time per exposure[2] and the minimum exposure time of 339 sec to avoid additional buffer dump overheads (see Pavlovsky et al. 2003), this means that three different fields can be observed per orbit, with $t_{\rm exp} = 8.5$ min at most. Figure 5 displays four optimal possibilities of where to choose such fields. The detection rate can therefore be tripled to finally get one lensing event every 5 days. Taking the risk of missing short events, one could also reduce the time sampling and measure 6 fields in periods of two HST orbits. Note that if the entire surface of Maffei 1 could be exploited, there would be over $2 \times 10^6$ useful stars.

For Gemini/NIRI, the total number of resolvable stars in Maffei 1 is $\int N_{\rm res} {\rm d}\Omega \approx 4 \times 10^5$. Hence even if the very short $t_{\rm exp}$ would allow to mosaic the full area covered by these stars, and assuming 10 h of observability per night, the detection rate would be only of one event every 8 days, somewhat less than with HST.

In classical lensing, the effective seeing is of crucial importance because it directly determines the number of resolvable stars. For instance, without adaptive optics and a seeing of 0.4″, NIRI would resolve only about $2 \times 10^4$ stars over all Maffei 1 at $Q_{\rm min} = 3$. Furthermore, NICMOS on HST, with its $K$-band diffraction limited effective seeing of 0.2″, would see about

[2] Unfortunately, the ACS field of view is too large to keep the same guide star when pointing toward adjacent fields; the overhead would be substantially less otherwise.

$6 \times 10^4$ stars at the same $Q_{\rm min}$ and could monitor only a tiny fraction of them. Hence, while high sensitivity does not really matter in the $K$-band here, large telescopes are nevertheless essential to alleviate the diffraction limit. Likewise, ground-based optical observations, which do not yet benefit from adaptive optic corrections, are hopeless at the moment for classical lensing searches.

However, one advantage of classical lensing over pixel lensing is that it does not suffer from non-photon noise, such as variable PSF, misalignment and pixelisation noise. In principle, classical lensing also always give access to the event timescales. To check for the non-chromatic dependence of the light curves would require observations with a second filter, which has been ignored here.

### 5.2. Pixel lensing

In pixel lensing, the source is not resolved and the noise is dominated by the stellar, sky plus instrumental background. The lensing events are revealed by subtracting a reference image ideally with no lensing event from the images with the ongoing events. The resulting difference images then show a PSF of the excess flux due to the lensing magnification. Neglecting the contribution of the excess flux to the noise, the signal-to-noise ratio in a difference image obtained from an exposure at time $t_i$ of an event with maximum magnification at time $t_0$ is:

$$Q_i = \frac{(\alpha F)[A(t_i; t_0, \beta, \omega) - 1]t_{\rm exp}}{\sqrt{\mu\Omega_{\rm psf}[(\alpha S) + (\alpha S_{\rm sky})]t_{\rm exp}}}, \tag{23}$$

where $t_{\rm exp}$ is the exposure time, $F$ the unamplified flux of the lensed star, $\mu$ a factor that takes into account the noise in the reference image, and $S$, $S_{\rm sky}$, $\Omega_{\rm psf}$ and $\alpha$ are as for Eq. (17). Note that in the absence of pixel noise, the subtraction performed when creating the difference image removes the fluctuation noise.

Now let's assume that the event is observed through $N$ exposures from time $t_1$ to time $t_2$, a time interval not necessary covering the entire event. The total signal-to-noise ratio of the measured portion of the event then is $Q = (\sum_{i=1}^{N} Q_i^2)^{1/2}$. In practice, an event is searched for by summing the difference images weighted by all possible and properly normalised $(A - 1)$ factors, intervening as a "filter" function. When the parameters of this factor coincide with those of the event, the signal-to-noise ratio of the event PSF on the summed image reaches a maximum with value given precisely by $Q$. If the exposures are taken uniformly at time intervals small relative to $\omega_{\rm eff}^{-1}$, and that the sky noise and the PSF remain constant with time, the sum in $Q$ can be converted into an integral yielding:

$$Q^2 = \frac{\pi\eta(\alpha F)^2}{\mu\Omega_{\rm psf}\left[(\alpha S) + (\alpha S_{\rm sky})\right]\omega}\frac{\zeta(t_0, \beta, \omega; t_1, t_2)}{\beta}, \tag{24}$$

$$\begin{aligned}\zeta(t_0, \beta, \omega; t_1, t_2) &\equiv \frac{\int_{t_1}^{t_2}\left[A(t; t_0, \beta, \omega) - 1\right]^2 {\rm d}t}{\beta^{-2}\int_{-\infty}^{\infty} G(t; t_0, \omega_{\rm eff})^2 {\rm d}t} \\ &= \frac{\omega\beta}{\pi}\left[2\left(1 - \frac{1}{\beta}\sqrt{\beta^2 + 4 - \frac{4}{1 + \frac{\beta^2}{\omega^2 t^2}}}\right)t + \frac{1}{\omega\beta}\cdot\right. \\ &\quad \left\{\arctan\left(\frac{\omega t}{\beta}\right) - \frac{\beta}{\sqrt{\beta^2 + 4}}\arctan\left(\frac{\omega t}{\sqrt{\beta^2 + 4}}\right)\right. \\ &\quad +2\beta\left[\sqrt{\beta^2 + 4}\,E\left(\frac{\omega t}{\sqrt{\omega^2 t^2 + \beta^2}}, \frac{2}{\sqrt{\beta^2 + 4}}\right)\right. \\ &\quad \left.\left.\left.-\frac{\beta^2 + 2}{\sqrt{\beta^2 + 4}}F\left(\frac{\omega t}{\sqrt{\omega^2 t^2 + \beta^2}}, \frac{2}{\sqrt{\beta^2 + 4}}\right)\right]\right\}\right]_{t_1 - t_0}^{t_2 - t_0}\end{aligned} \tag{25}$$

where $\eta \equiv Nt_{\rm exp}/(t_2 - t_1)$ is the time fraction really dedicated to observe the source galaxy, and $F(z, k)$ and $E(z, k)$ are the incomplete elliptical integrals of the first and second kind respectively. The function $\zeta$ is always $\leq 1$. In the case where $t_1 \to -\infty$ and $t_2 \to \infty$, it depends only on $\beta$ and coincides with the monotonically decreasing suppression function defined in G96, with $\zeta \to 1$ for $\beta \ll 1$.

Only the lensing events above a given signal-to-noise threshold, say $Q > Q_{\rm min}$, are detectable. For given $F$, $\omega$ and $t_0$, this condition and Eq. (24) define a maximum impact parameter $\beta_{\rm max}(F, t_0, \omega; t_1, t_2)$ as the solution for $\beta$ of:

$$\frac{\beta}{\beta_{\rm max}^{\circ}(F)} = \zeta(t_0, \beta, \omega; t_1, t_2), \tag{26}$$

$$\beta_{\rm max}^{\circ}(F) = \frac{\pi\eta(\alpha F)^2}{Q_{\rm min}^2\mu\Omega_{\rm psf}[(\alpha S) + (\alpha S_{\rm sky})]\omega}, \tag{27}$$

such that events with larger impact parameters will not be detected. As mentioned in Sect. 3.2, there also exists a lower limit for the impact parameter owing to the finite radius of the stellar sources, below which the magnification is less than predicted by Eq. (1). For simplicity, we will assume that there is a one-to-one relation between the stellar radius $R_{\rm S}$ and the flux, and in particular that $R_{\rm S}$ does not depend on colour. A justification for this assumption is that elliptical galaxies like Maffei 1 essentially contain old stellar populations and thus the bright end of their stellar luminosity function is dominated by red giants spanning a rather small colour range. From Stefan-Bolzmann's law it then follows that $R_{\rm S} = R_{\rm lim}10^{-(M - M_{\rm lim})/5}$, where $M$ is the absolute magnitude of the star and $R_{\rm lim} \approx 100\ R_{\odot}$ the stellar radius at the tip of the red giant branch. In this form, our approximation is most accurate for the brightest stars, which are the main sources contributing to observable lensing events, and will overestimates the derived minimum impact parameter for fainter stars. Keeping only events with $\beta \geq 0.5\theta_{\rm S}/\theta_{\rm E}$ thus implies:

$$\beta_{\rm min}(F) = \frac{1}{2}\frac{D_{\rm L}}{r_{\rm E}}\frac{R_{\rm lim}10^{-M/5}}{D_{\rm S}}\cdot \tag{28}$$

The number of detectable events from a star with peak magnification between times $t_0$ and $t_0 + {\rm d}t_0$ then simply is $\Delta\beta\,\Gamma_0{\rm d}t_0$, where:

$$\Delta\beta(F, t_0, \omega; t_1, t_2) \equiv \max(\min(\beta_{\rm max}, 1) - \beta_{\rm min}, 0) \tag{29}$$

and $\Gamma_0$ is the classical event rate given by Eq. (21). The upper limit of 1 is introduced in Eq. (29) to exclude events with $\beta > 1$, which by definition do not contribute to the microlensing optical depth.

Finally, the total number of detectable events within the observing time from $t_1$ to $t_2$ and per unit solid angle is obtained by multiplication with the stellar surface density $S/\int_0^\infty \Phi(F)F\mathrm{d}F$ and by integration over the luminosity function and over the magnification peak times:

$$N_{\rm det} = \frac{2}{Q_{\rm min}^2}\frac{\eta}{\mu}\cdot\tau\frac{(\alpha F^*)}{\Omega_{\rm psf}}\frac{(\alpha S)}{(\alpha S)+(\alpha S_{\rm sky})}\int_{-\infty}^{\infty}\xi\,\mathrm{d}t_0, \quad (30)$$

$$\xi(t_0,\omega;t_1,t_2) = \frac{\int_0^\infty \Phi(F)\Delta\beta(F,t_0,\omega;t_1,t_2)\mathrm{d}F}{\int_0^\infty \Phi(F)\beta_{\rm max}^2(F)\mathrm{d}F}. \quad (31)$$

In addition to this detection number, it is also useful to know what fraction of the detected events will have a measurable timescale. For this purpose, we use the statistical procedure describe in Gould (1995a). The rate of electrons produced on the detector by a lensed source star follows the distribution:

$$\mathcal{F}(t;F,t_0,\beta,\omega) = \eta(\alpha F)[A(t,t_0,\beta,\omega)-1]+B, \quad (32)$$

where $B = \eta\{(\alpha F)+\Omega_{\rm psf}[(\alpha S)+(\alpha S_{\rm sky})]\}$ is the background rate including the unmagnified flux from the star. This background can be accurately determined from data taken outside the lensing event, like the reference images. Noting $\lambda_i$, $i = 1,..,4$, the free parameters $F$, $t_0$, $\beta$ and $\omega$, the covariance matrix of these parameters can be calculated as:

$$\mathrm{cov}(\lambda_i,\lambda_j) = \{b^{-1}\}_{ij}, \quad (33)$$

$$b_{ij} \equiv \int_{t_1}^{t_2}\mathcal{F}(t;F,t_0,\beta,\omega)\frac{\partial\ln\mathcal{F}}{\partial\lambda_i}\frac{\partial\ln\mathcal{F}}{\partial\lambda_j}\mathrm{d}t, \quad (34)$$

and thus $\delta\omega^2 = \mathrm{cov}(\omega,\omega)$. At each apparent radius of the source galaxy, the sub-number $\Delta N_{\rm det}(\delta w/w \le \varepsilon)$ of events with $\delta w/w \le \varepsilon$ is then computed in the same way as for $N_{\rm det}$, except that $\beta_{\rm max}$ is replaced by the impact parameter where $\delta w/w = \varepsilon$.

We will now estimate $N_{\rm det}$ for observations made with a selection of telescope and instrument combinations within a period $\Delta t = t_2 - t_1 = 10$ h, i.e. the typical duration of a ground-based observing night, assuming the conditions and properties listed in Table 2. The observing overheads, i.e. $(1-\eta)$, are estimated assuming that a single field is observed and hence no repeated telescope pointings and guide star acquisitions are needed. For HST/ACS, in addition to the 40 min of non-visibility time per orbit, the overheads then amount to $9.7 + 2.5\cdot(\mathcal{N}-1)$ min per orbit plus 0.4 min for the first orbit, where $\mathcal{N}$ is the number of exposures per orbit (see Pavlovsky et al. 2003). This number is constrained by the detector saturation, which for ACS and the central surface brightness of Maffei 1 is reached after ~20 min integration[3]. To ensure some margin for high lensing amplification, we choose $\mathcal{N} = 4$ and $t_{\rm exp} = 9.7$ min, representing a total overhead of about 60%. For Gemini/NIRI, the overhead is about 25% according to the instrument web pages, and the same overhead is taken for all other ground-based means. No time is reserved for sky frames and chopping, as the effect of variable sky and fringes is not expected to hide and significantly perturb the photometry of the PSFs on the difference images, and for exposures with other filters. The reference images are assumed to be obtained from a similar set of observations taken on another night, preferably at a few days interval to completely erase the trace of presumed events, so that $\mu = 2$ (see also Sect. 9.6 in G96). Although this procedure doubles the required observing time, it also doubles the number of detectable events since the role of the event and reference images can be interchanged.

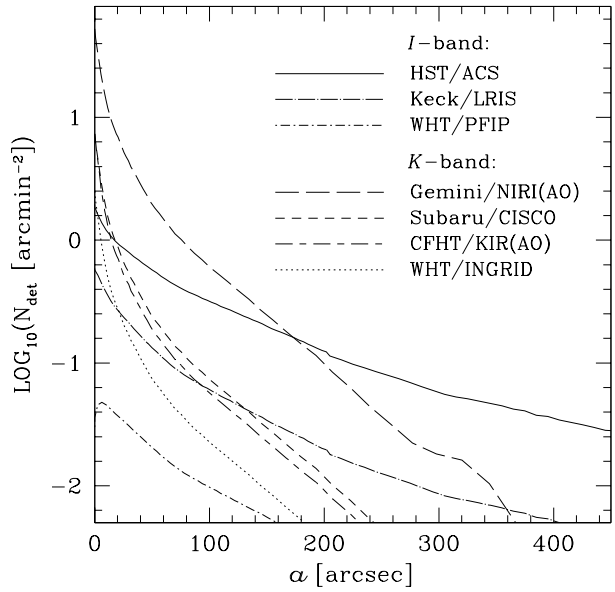


**Fig. 6.** Expected number of detectable pixel lensing events per arcmin$^2$ in Maffei 1 as a function of angular radius $a$ along the galaxy major axis, when observing 10 h with various combinations of telescopes and detectors, and for the surface brightness profiles displayed in Fig. 2. The signal-to-noise threshold is $Q_{\rm min} = 5$, and AO indicates the use of adaptive optics. The observing parameters are specified in Table 2.

Figure 6 plots the resulting radial profiles of $N_{\rm det}$ for $Q_{\rm min} = 5$. The first thing to notice is that, contrary to classical lensing, all the curves peak near the centre. Since the non-integral part of $N_{\rm det}$ in Eq. (30) is also directly proportional to $\eta$ and the curves rapidly decline with radius, it is therefore best to rely on a single field at the centre of Maffei 1, hence justifying our overhead calculations. Moreover, the size of the field of view is not as limiting as in classical lensing, because the dominant contribution to the event detection rates comes from the innermost regions.

A second point is that, again unlike classical lensing, adaptive optics (AO) is not an absolute prerequisite for pixel lensing searches. As an example in the $K$-band, Subaru/CISCO without AO can detect more events (over the entire detector *and* per unit area) than CFHT/KIR with AO. In particular, this means that ground-based optical observations can also efficiently chase pixel lensing events. In fact, in the point source limit ($\beta_{\rm min} = 0$) and for fully measured light curves ($t_1 \to -\infty$ and $t_2 \to +\infty$), the detection rate integrated over the solid angle $\Omega$ covered by the detector *increases* with increasing effective

[3] Taking a detector gain larger than the default value of 1 would allow a longer integration time.

**Table 2.** Characteristics of some telescope plus instrument combinations, and the resulting expected total number of pixel lensing events $\int N_{\rm det}{\rm d}\Omega$ over the full field of view with a total signal-to-noise ratio $Q \geq 5$ and the fraction $p(\delta w/w \leq 0.5)$ of these events with timescales measurable at a precision better than 50%, when observing the central region of Maffei 1 in a 10 h program and assuming pre-existing reference images at the same noise level as the event images. More precisely, $p(\delta w/w \leq \varepsilon) \equiv \int \Delta N_{\rm det}(\delta w/w \leq \varepsilon){\rm d}\Omega / \int N_{\rm det}{\rm d}\Omega$. AO stands for instruments in adaptive optic mode. $Z$ is the telescope zeropoint magnitude yielding 1 $e^-$/s, and $S_{\rm sky}$ the background comprising the sky and any instrumental background not related to the observed galaxy. The adopted values refer to data found on the instrument web pages (except for Keck and WHT $I$-band backgrounds). The seeing $\theta_{\rm see}$ represents the full width at half maximum of the point spread function. For the HST, the value is taken from Buta & McCall 2003. With AO, the diffraction limit $\theta_{\rm see} \approx 1.22\lambda/D$, where $D$ is the telescope diameter, is adopted, and otherwise the median site seeing $\theta_{\rm see} \approx 0.7''(\lambda/[0.5\,\mu{\rm m}])^{-1/5}$, valid for Mauna Kea and La Palma, is assumed.

| Telescope/instrument | Filter | $Z$ (mag for 1 $e^-$/s) | $S_{\rm sky}$ [mag/arcsec$^2$] | $\theta_{\rm see}$ [arcsec] | Field of view [arcsec$^2$] | $\int N_{\rm det}{\rm d}\Omega$ | $p(\delta w/w \leq 0.5)$ [%] |
|---|---|---|---|---|---|---|---|
| HST/ACS | $I$ | 25.5 | 21.43 | 0.076 | $202 \times 202$ | 5.11 | 3.9 |
| Keck/LRIS | $I$ | 28.0 | 19.5 | 0.63 | $360 \times 468$ | 1.92 | 2.5 |
| WHT/PFIP | $I$ | 25.6 | 19.5 | 0.64 | $972 \times 972$ | 0.46 | 0 |
| Gemini/NIRI(AO) | $K$ | 26.1 | 13.75 | 0.070 | $51 \times 51$ | 6.32 | 8.7 |
| Subaru/CISCO | $K$ | 26.1 | 12.7 | 0.52 | $108 \times 108$ | 1.54 | 6.1 |
| CFHT/KIR(AO) | $K$ | 24.0 | 11.6 | 0.154 | $36 \times 36$ | 0.53 | 5.6 |
| WHT/INGRID | $K$ | 24.5 | 12.0 | 0.52 | $244 \times 244$ | 0.76 | 3.9 |

seeing if the focal length of the telescope is adjusted in a way such that $\Omega$ scales as $\Omega_{\rm psf}$ and if $N_{\rm det}$ remains uniform within the field of view. Indeed, under these assumptions, $\xi$ gets independent of $t_0$ and $\omega$ and $\int [N_{\rm det}/\Delta t]{\rm d}\Omega \propto \Omega/\Omega_{\rm psf}\xi$, and since the suppression function $\zeta$ reduces to a monotonically decreasing function of $\beta$, Eqs. (26) and (27) imply that $\beta_{\rm max}/\beta^{\circ}_{\rm max}$ and therefore $\xi$ increase with $\Omega_{\rm psf}$. When reaching the spike regime (see Sect. 3.1), $\beta_{\rm max} \rightarrow \beta^{\circ}_{\rm max}$ and $\xi \approx 1$. In this case, the decrease of the detectable event cross section per source star, i.e. the area of the $\beta \leq \beta_{\rm max}$ disc, is exactly compensated by the increase of the number of such stars within the field of view.

In practice, however, the gradual increase of the detection rate with $\Omega_{\rm psf}$ at a constant number of resolution elements $\Omega/\Omega_{\rm psf}$ is limited by the finite size of the stellar sources and of the target galaxy. The finite source effect is illustrated for example in Fig. 6 by the WHT/PFIP case, where the growth of $N_{\rm det}$ with increasing surface brightness reverses near the center because $\beta_{\rm max}$ approaches the $\beta_{\rm min}$ limit. For observations by large telescopes in the $K$-band, this limit is not reached and thus $N_{\rm det}$ does not depend on our rough evaluation of $\beta_{\rm min}$. Note also that $\omega_{\rm eff}^{-1}$ decreases with $\beta$, which means that an improved time resolution is needed at degrading spatial resolution.

According to Fig. 6, the number of detections in the central region of Maffei 1 is superior for ground-based 8 m-class telescopes in the $K$-band than for HST in the $I$-band, but $N_{\rm det}$ declines faster with radius in the $K$-band than in the $I$-band. Table 2 gives the total number of $5\sigma$ event detections when pointing the galaxy centre and integrating $N_{\rm det}$ plotted in Fig. 6 over the field of view of the detectors, which is the truly relevant quantity to inter-compare the capabilities of the various observing means, as well as the fraction of detections where the timescale can be inferred with a precision better than 50%. The predicted detection numbers are quite substantial, with over 10 events for Gemini North and for HST if one takes into account the factor 2 gained by interchanging the role of the source and reference images. Even the other telescopes should all yield of order one or more detections per double night. However, the timescales may reasonably be accessed only by the largest telescopes with AO in the $K$-band. In particular, Gemini North should provide about one timescale at the 50% precision level every two nights.

Note that according to the terminology and the $F_{\rm max}$ versus $F_*$ criteria developed in G96, pixel lensing of the central region of Maffei 1 falls in the spike regime for WHT/PFIP, in the semiclassical regime for HST/ACS, at the transition between the two regimes for Keck/LRIS, and in the semiclassical regime for all $K$-band observing facilities considered here.

The so far computed detection numbers are based on $D_{\rm L} = 10$ kpc, $v = 50$ km s$^{-1}$ and $m_{\rm L} = 1\ M_{\oplus}$, implying $\omega^{-1} = 13$ h. The weak dependence of the timescale on $D_{\rm L}$ in the context of circular motion has already been highlighted in Sect. 3.4, and Eq. (30) reveals that $N_{\rm det}$ depends on $\omega$ only via the $\xi$ integral, which in the spike regime limit is also independent of $\omega$. If $D_{\rm L} = 3$ kpc while keeping $v$ and $m_{\rm L}$ at the same default values, the $\int N_{\rm det}{\rm d}\Omega$ listed in Table 2 change to 6.2 for HST/ACS and to 7.3 for Gemini/NIRI, showing that our rather large default choice of $D_{\rm L}$ in fact underestimates the true number of detections. If now $v = \{25, 100\}$ km s$^{-1}$ while keeping the other parameters at their default values, these numbers become respectively $\{4.6, 6.0\}$ for HST/ACS and $\{5.9, 7.4\}$ for Gemini/NIRI. These examples illustrate that introducing a distance and a velocity distribution of the $H_2$ cores in our pixel lensing detection calculation will not modify much the reported results.

The effect of varying $m_{\rm L}$ is two-folded. Firstly, $\omega^{-1} \propto \sqrt{m_{\rm L} D_{\rm L}}/v$ and therefore this parameter acts the same way as $D_{\rm L}$, producing a modest increase of $\int N_{\rm det}{\rm d}\Omega$ at decreasing $m_{\rm L}$. Secondly, $\beta_{\rm min} \propto r_{\rm E}^{-1} \propto m_{\rm L}^{-1/2}$, thus $\beta_{\rm min}$ rises with decreasing $m_{\rm L}$ and as a consequence $N_{\rm det}$ diminishes. This decrease becomes important especially when $\beta_{\rm min}$ gets close to $\beta_{\rm max}$, which first happens at the galaxy centre. The net effect at decreasing $m_{\rm L}$ is that $\int N_{\rm det}{\rm d}\Omega$ passes through a maximum of 5.4 events at $m_{\rm L} \approx 0.2\ M_{\oplus}$ for HST/ACS, and of 11.2 events at $m_{\rm L} \approx 0.006\ M_{\oplus}$ for Gemini/NIRI, and $N_{\rm det}$ starts to vanish at the centre at $m_{\rm L} \approx 0.02\ M_{\oplus}$ for HST and $0.0008\ M_{\oplus}$ for Gemini. The number of detections does not depend much

on the mass spectrum as long as most lenses have masses above these critical values. However, at $m_L = 0.001\ M_\oplus$, the timescale is only ~50 min, requiring high frequency sampling.

If one includes those events with $\beta_{max} > 1$, i.e. releases the lower limit of 1 in Eq. (29), then $\int N_{det} d\Omega = 5.2$ for HST/ACS and 8.3 for Gemini/NIRI. The gain is larger in the second case because the events have larger $\beta$ at fixed value of $Q$. If now the detection threshold is set to $Q_{min} = 7$, then $\int N_{det} d\Omega$ would be 3.3 for HST/ACS and 4.9 for Gemini/NIRI.

As the timescale decreases, the fraction of event with $\delta w/w \leq 0.5$ increases because a larger portion of the light curve is probed within the fixed observing time window $\Delta t$. To illustrate this, taking $v = 100\ km\ s^{-1}$ reduces the timescale by a factor of two and transforms the values of $p(\delta w/w \leq 0.5)$ given in Table 2 to 9.3% for HST/ACS and to 18.6% for Gemini/NIRI.

It should be noted that the $51'' \times 51''$ field of view assumed for NIRI/AO relies on the non-conventional but practically possible f/14 camera mode. In the normal f/32 mode, the field of view would be only $22'' \times 22''$. Although optimal PSF sampling is not a necessity for pixel lensing, at f/14, $\Omega_{psf}$ is still sampled by 6 pixels in the $K$-band. In all other selected telescope and instrument combinations, the sampling is at least as good. Figure 5 also displays some possible AO guide stars. The central grey dot is in fact a 12.1 mag compact nuclear source with an intrinsic full width at half maximum of 0.080″ (Buta & McCall 2003), and represents an acceptable option. Otherwise, the best point source appears to be the 12.3 mag star located 25″ south-west from the galaxy centre. One pitfall of the current Gemini North AO system, which explains the avoidance of the NIRI f/14 mode, is a degradation of the image quality beyond ~10″ from the guide star. If this is a problem, one may still resort to the IRCS instrument on the Subaru telescope, with a $58'' \times 58''$ field of view and where the AO ensures a good image quality within 30″ from the guide star.

Finally, regarding the noise induced by systematic effects (time-variable PSF, photometric and geometric misalignments and discrete pixelisation), G96 has shown that it can always be reduced below the photon noise. Clearly, observations from space are free of airmass constraints, and in particular will be less affected by variable PSF and image distortion problems.

## 6. Constraints from microlensing experiments

The EROS and MACHO collaborations (Alcock et al. 1998) have published combined limits on the number of planetary-mass dark matter objects in the Galactic halo from their classical microlensing surveys of the Magellanic Clouds, relying on halo models more spherical than an ellipticity of E6. For halos composed entirely of Earth-mass objects, they predict up to 100 lensing events whereas none was found, and more generally, they conclude that objects with $3.5 \times 10^{-7} < m_L/M_\odot < 4.5 \times 10^{-5}$ make up less than 10% of the total dark halo mass.

This does not rule out the possible existence of massive $H_2$-core discs in the Milky Way and the LMC. Indeed, in the case of LMC searches, $D_S \approx 55$ kpc and typical lens distances and transverse velocities are $D_L = 15$ kpc and $v \sim 175\ km\ s^{-1}$ for halo lenses (Renault et al. 1998), $D_L \sim 0.5$ kpc and $v \sim 50\ km\ s^{-1}$ for Galactic $H_2$ lenses, and $(D_S - D_L) \sim 0.3$ kpc and $v \sim 30\ km\ s^{-1}$ for LMC $H_2$ lenses (Gyuk et al. 2000), so that at given lens mass, $\omega^{-1} \propto [D_L(D_S - D_L)]^{1/2}/v$ does not vary much more than ~50% among these different lens phase-space distributions. Hence the classical detection rates, as given by Eq. (21), depend predominantly on the optical depths.

For a traditional roundish Galactic dark halo full of compact lenses, $\tau \approx 5 \times 10^{-7}$. For Galactic $H_2$ cores with $\gamma = 2$ times the mass density of the HI distribution, assuming that the HI has a Gaussian vertical distribution with standard deviation $\sigma$ and local surface density $\Sigma$ and that the Sun sits in the middle of the Galactic plane, one gets:

$$\tau = \frac{2\sqrt{2\pi} G \gamma \Sigma \sigma}{c^2 \sin^2 b}. \quad (35)$$

The Galactic latitude of the LMC is $b \approx -33°$, and taking $\sigma = 300$ pc and $\Sigma = 5\ M_\odot/pc^2$, the result is $\tau = 2.4 \times 10^{-9}$. For $H_2$ cores in the LMC disc, the optical depth must be averaged over the stellar sources in this disc. Assuming the same $\gamma$ factor as for the Milky Way, a Gaussian vertical distribution of the LMC HI gas with $\sigma = 180$ pc and an average $\Sigma/\cos i = 22.4\ M_\odot/pc^2$ (Kim et al. 2003), where $i \approx 35°$ is the inclination angle of the LMC disc from face-on, and an exponential vertical stellar distribution with a scale height of 300 pc (Gyuk et al. 2000), one finds $\tau = 5.1 \times 10^{-9}$. Hence the microlensing optical depths of $H_2$ cores in the Milky Way disc and in the LMC disc are in both cases two orders of magnitude less than in the case of lenses distributed in a more spherical halo, rendering the expected detection number of such cores consistent with the reported non-detection of Earth-mass lenses.

A similar argument also holds for pixel lensing experiments targeting M 31. Indeed, the predicted optical depth towards this galaxy due to ~spherical dark halos of compact objects around both the Milky Way and Andromeda is $\tau \approx (5-10) \times 10^{-6}$ (e.g. Crotts 1992) and predicted lensing rates for $10^{-3} \lesssim m_L/M_\odot \lesssim 1$ reach about 200 event per year (Kerins et al. 2001; Han 1996), while the optical depth of Galactic disc $H_2$ cores towards M 31 is similar to that inferred towards the LMC. According to Sect. 5.2, $\Gamma \sim \tau \cdot \xi$. When passing from $(0.01-1)\ M_\odot$ halo lenses to Earth-mass Galactic $H_2$-core lenses, $\tau$ decreases by over 3 orders of magnitude whereas $\xi$ increases by no more than a factor of ~20, because $\xi \sim \Delta\beta/\beta^\circ_{max} \leq \zeta$ and $\zeta$ increases from ~0.05 to 1 when $\beta$ goes from 1 to 0 if $t_1 \to -\infty$ and $t_2 \to +\infty$. The last inequality particularly reflects the non-zero $\beta_{min}$ value. Hence the detection rate of $H_2$ cores falls by a factor $\gtrsim$100, as for the LMC experiments.

The MEGA microlensing team (Alves et al. 2001) has attempted to put limits on low-mass halo objects from a high time-resolution survey of M 31 using the Subaru telescope, which unfortunatley encountered bad weather. For halos with 100% earth-mass objects, they predict about 60 events in two nights. If the lenses were $H_2$-cores in the Galactic disc, this rate would reduce to roughly 0.1 event per night, well below the sensitivity of equivalent searches towards Maffei 1.

An important point is that by symmetry the absolute Einstein radius is similar for lenses in the Milky Way and lenses in the source galaxy. Referring to Eq. (28), this means in particular that $\beta_{min} \propto D_L$ and therefore the low-mass lenses in a

distant source galaxy will have a negligible detection rate relative to the local ones.

## 7. Conclusion

The theory of cold $H_2$ globules with condensed central cores to account for dark matter in spiral galaxies can be readily tested by microlensing. If such globules exist in the Milky Way, the previous microlensing experiments have looked in directions that do not optimise their detection rates. These globules are indeed expected to follow the HI distribution and should be concentrated in the outer Galactic disc, where the contribution of invisible mass is highest. The large galaxies in the Maffei group provide excellent microlensing targets to probe the $H_2$-core content of this region. In particular, the Maffei 1 elliptical is at a distance of only 3 Mpc, very close to the Galactic plane and ∼44° away from the Galactic anti-centre, and offers a huge reservoir of microlensing sources.

The condensed $H_2$-globule cores have mass and size comparable to the Earth or less. The Earth-mass Galactic $H_2$ core-Maffei 1 lensing geometry implies an Einstein radius of $\sim 3\ R_\odot$, large enough to consider the source stars as point-like over a large range of impact parameters. Assuming that the $H_2$ cores are distributed with twice the HI mass density, the microlensing optical depth towards Maffei 1 of these cores is $\tau \approx 0.7 \times 10^{-6}$, and in the circular orbit approximation, the typical timescale of the lensing events is at most ∼1 day.

In the classical lensing approach, due to the fluctuation noise, the surface density of resolvable stars in Maffei 1 as a function of apparent major-axis radius $a$ peaks away from the centre, at $a \approx 230$ arcsec in the $I$-band and at $a \approx 90$ arcsec in the $K$-band, and high resolution is crucial to maximise the amplitude of this peak. Because of the smaller Maffei 1 area with a high density of resolvable stars and the restricted detector size in the $K$-band, and of the poor seeing in ground-based optical observations, the ACS camera on HST is currently the only useful instrument. In the $I$-band and monitoring several fields at the same time, it would take ∼5 days of ACS observations to detect one event.

The pixel lensing approach, however, is over one order of magnitude more efficient. In this case, the detection rate is maximum in the central region ($a = 0$) and it is best to rely on a single field centred at this position. Since pixel lensing involves the subtraction of reference images from the images with the ongoing lensing events, at least two observing runs are required, spaced by a time interval large relative to the lensing timescale, to get the two sets of images. The roles of the reference and event images can fortunately be interchanged to double the number of detectable events. We find that in the $K$-band and resorting to adaptive optics, the ground-based 8 m-class telescopes could detect as many as 10 events at the $5\sigma$ level in two nights, and that in the $I$-band, the ACS camera could detect a similar number of events at the same threshold in two 10-h observing periods.

About 9% of the events detected by 8 m-class telescopes in $K$ should have timescales measurable at a precision better than 50%, representing about one such timescale per pair of nights, while this fraction reduces to ∼4% for the ACS observations in $I$. A potentially powerful way to constrain the typical lens mass $m_\mathrm{L}$ could be to measure the event detection rate as a function of the radius $a$. Indeed, the average impact parameter of detectable events decreases with increasing galaxy surface brightness, and the finite radius of the source stars imposes a lower limit $\beta_\mathrm{min} \propto m_\mathrm{L}^{-1/2}$ below which the true flux amplification becomes much less than the point-source approximation. As a consequence, the detection rate curve will display a maximum at a radius related to the lens mass, with its precise location depending on the signal-to-noise threshold.

The advent of instruments like WEBCam on JWST in the near-IR, with a field of view of $2.16' \times 2.16'$, will boost the detection numbers derived here. Although a positive detection will not yet prove that the intervening lens is an $H_2$ core, it will certainly represent a significant step towards understanding the origin of dark matter, whereas a no-detection result may refute the cored $H_2$ globules as a representative mass constituent of the Galaxy.

*Acknowledgements.* The author is grateful to André Blecha for his information regarding observational aspects with large telescopes, and to Eamonn Kerins for referring the paper.

## References

Afonso, C., Albert, J. N., Alard, C., et al. 2003, A&A, 404, 145
Alcock, C., Allsman, R. A., Alves, D., et al. 1998, ApJ, 499, L9
Alcock, C., Allsman, R. A., Alves, D., et al. 2001, ApJS, 136, 439
Alves, D. R., Baltz, E. A., Crotts, A., et al. 2004, in Dark Matter in Galaxies, ed. S. Ryder, D. J. Pisano, M. Walker, & K. Freeman (San Francisco: ASP), IAU Symp. 220, 127
Bond, I. A., Abe, F., Dodd, R. J., et al. 2001, MNRAS 327, 868
Bosma, A. 1981, AJ, 86, 1825
Burton, W. B. 1992, in Saas-Fee Advanced Course 21, Galactic Interstellar Medium, ed. D. Pfenniger, & P. Bartholdi (Springer-Verlag), 21
Burton, W. B., & Liszt, H. S. 1978, ApJ, 225, 815
Buta, R. J., & McCall, M. L. 1999, ApJS, 124, 33
Buta, R., & McCall, M. L. 2003, AJ, 125, 1150
Cantiello, M., Raimondo, G., Brocato, E., & Capaccioli, M. 2003, AJ, 125, 2783
Crotts, A. P. S. 1992, ApJ, 399, L43
Cuillandre, J.-C., Lequeux, J., Allen, R. J., Mellier, Y., & Bertin, E. 2001, ApJ, 554, 190
de Jong, J. T. A., Kuijken, K., Crotts, A. P. S., et al. 2004, A&A, 417, 461
Fingerhut, R. L., McCall, M. L., Robertis, M. D., et al. 2003, ApJ, 587, 672
Gould, A. 1995a, ApJ, 440, 510
Gould, A. 1995b, ApJ, 455, 44
Gould, A. 1996, ApJ, 470, 201 (G96)
Gyuk, G., Dalal, N., & Griest, K. 2000, ApJ, 535, 90
Han, C. 1996, ApJ, 472, 108
Hartmann, D., & Burton, W. B. 1997, in Atlas of Galactic Neutral Hydrogen (New York: Cambridge Univ. Press)
Holtzman, J. A., Watson, A. M., Baum, W. A., et al. 1998, AJ, 115, 1946
Jarrett, T. H., Chester, T., Cutri, R., Schneider, S., & Huchra, J. P. 2003, AJ, 125, 525
Jensen, J. B., Tonry, J. L., Barris, B., et al. 2003, ApJ, 583, 712
Karachentsev, I. D., Sharina, M. E., Dolphin, A. E., & Grebel, E. K. 2003, A&A, 408, 111

Kerins, E., Carr, B. J., Evans, N. W., et al. 2001, MNRAS 323, 13
Kerr, F. J., Bowers, P. F., Kerr, M., & Jackson, P. D. 1986, A&AS, 66, 373
Kim, S., Staveley-Smith, L., Dopita, M. A., et al. 2003, ApJSS, 148, 473
Liu, M. C., Graham, J. R., & Charlot, S. 2002, ApJ, 564, 216
Melchior, A.-L., Afonso, C., Ansari, R., et al. 1998, A&A, 339, 658
Paulin-Henriksson, S., Baillon, P., Bouquet, A., et al. 2003, A&A, 405, 15
Pavlovsky, C., Biretta, J., Boffi, F., et al. 2003, ACS, Instrument Handbook, version 4.0. (Baltimore: STScI)
Pfenniger, D. 2004, A&A, in preparation. See also:
(i) Pfenniger, D. 2004, in Recycling Intergalactic and Interstellar Matter, ed. P.-A. Duc, J. Braine, & E. Brinks (San Francisco: ASP), IAU Symp. 217, 228;
(ii) Pfenniger, D. 2004, in IAU Symp., ed. S. D. Ryder, D. J. Pisano, M. A. Walker, & K. C. Freeman (San Francisco: ASP), 220, 241
Pfenniger, D., & Combes, F. 1994, A&A, 285, 94
Popowski, P., Vandehei, T., Griest, K., et al. 2001, in Astrophysical Ages and Time Scales, ed. T. von Hippel, N. Manset, & C. Simpson, ASP Conf. Ser. 245, 358
Rafikov, R. R., & Draine, B. T. 2001, ApJ, 547, 207
Renault, C., Aubourg, É., Bareyre, P., et al. 1998, A&A, 329, 522
Revaz, Y., & Pfenniger, D. 2004, A&A, 425, 67
Riffeser, A., Fliri, J., Bender, R., Seitz, S., Gössl, C. A. 2003, ApJ, 599, 17
Rogstad, D. H., & Shostak, G. S. 1972, ApJ, 176, 315
Terndrup, D. M., Frogel, J. A., & Whitford, A. E. 1990, ApJ, 357, 453
Tiede, G. P., Frogel, J. A., & Terndrup, D. M. 1995, AJ, 110, 2788
Tonry, J. L., Blakeslee, J. P., Ajhar, E. A., & Dressler, A. 1997, ApJ, 475, 399
White, R. S. 1996, Ap&SS 240, 75
Wozniak, P. R., Udalski, A., Szymanski, M., et al. 2001, AcA 51, 175